Journal of Constructional Steel Research 155 (2019) 46–61

Contents lists available at ScienceDirect

Journal of Constructional Steel Research

Experimental investigation on sea sand concrete-filled stainless steel tubular stub columns

Fei-Yu Liao [a], Chao Hou [b,*], Wei-Jie Zhang [a], Jie Ren [b]

[a] College of Transportation and Civil Engineering, Fujian Agriculture and Forestry University, Fuzhou, 350002, PR China
[b] School of Civil Engineering, The University of Sydney, Sydney, NSW 2006, Australia

ARTICLE INFO

Article history:
Received 14 November 2018
Received in revised form 14 December 2018
Accepted 14 December 2018
Available online xxxx

Keywords:
Sea sand concrete
Stainless steel
Concrete-filled stainless steel tube (CFSST)
Experimental behaviour
Strength prediction

ABSTRACT

This paper studies the behaviour of sea sand concrete-filled stainless steel tube (CFSST) stub columns under axial compression through experimental investigations. A total of 48 specimens were tested, including circular and square stainless steel tubes filled with three types of core concrete, including natural river sand concrete, desalted sea sand concrete and natural sea sand concrete. The effects of key parameters such as the tubular thickness of stainless steel, the cross-sectional configuration and the types of concrete infill on the behaviour of these innovative composite columns were investigated. The confinement effects of CFSST with sea sand concrete were evaluated and compared with that of CFSST with conventional river sand concrete. Testing results showed that the tested CFSST columns showed generally high strength and excellent ductility, while the confinement effect of stainless steel on the sea sand concrete is as reliable as that on the river sand concrete counterpart. Comparisons were made between the test results and the predicted ultimate sectional capacity using the existing specifications AISC360–10 (2010), EC4 (2004) and DBJ/T13-51-2010 (2010). These codes are proved reasonably conservative for predicting the sectional strength of sea sand concrete-filled stainless steel tubular stub columns.

1. Introduction

Concrete-filled steel tubes (CFST) incorporate an encasing steel tube and core concrete which acts together to improve the overall structural behavior. Numerous advantages of the two materials can be encompassed in CFST structural members to achieve enhanced bearing capacity, higher stability and stiffness, improved ductility and better energy absorption capacities, compared to those of traditional reinforced concrete (RC) or steel members [1–3]. It is believed that the above-mentioned enhancements mainly attribute to the composite action and confinement effect between the steel and concrete material [4,5]. According to previous studies, the confinement effect is dominated by a few factors including the steel tubular dimension and thickness, the concrete strength, the yield stress of steel and the column cross-sectional configuration [1,6,7]. To quantitatively address the passive confinement of carbon steel tube on its core concrete, a confinement factor (ξ) was defined as $A_s f_y / A_c f_{ck}$ in [1], where A_s is the cross-sectional area of steel tube; f_y is the yield strength of steel; A_c is the cross-sectional area of concrete and f_{ck} is the characteristic compressive strength of the core concrete.

Due to the structural advantages described above, CFST has been widely used over the past few decades in the construction industry, leading to a sequentially growing demand for the relevant resources [8,9]. As a matter of fact, since concrete material is extensively consumed in construction, the natural river sand has been overexploited to be used as the fine aggregates, causing its decreasing replenishment and further ecological imbalances [10]. In some coastal areas, freshwater sand resources are running out due to the continued massive consumption, whilst the sand transportation can further increase the cost of fine aggregates by at least 10% [11]. In such cases, the utilization of sea sand in replace of traditional river sand in concrete preparation makes a potential solution in alleviating the current contradiction between the limited river sand resource and the increasing demand for fine aggregates. Although it is concerned that the excessive use of sea sand concrete might lead to potential quality risks in past practices, many researchers believe that the sea sand concrete can be appropriately utilized if its structural properties are fully understood and proper construction measures are taken [8,10–11].

It can be easily deduced that, when the conventional river sand concrete is replaced by the sea sand concrete, a considerably high composition of chloride iron, shell and lightweight impurities would be introduced and thus lead to high corrosion risk for the conventional carbon steel tube or reinforcement. To solve this problem, the adoption of stainless steel tube becomes feasible since it has high corrosion

* Corresponding author.
E-mail address: chao.hou@sydney.edu.au (C. Hou).

https://doi.org/10.1016/j.jcsr.2018.12.009
0143-974X/

Nomenclature

A_c	Cross-sectional area of the concrete
A_s	Cross-sectional area of the stainless steel tube
B	Outer width of the square stainless steel tube
CFST	Concrete-filled steel tube
CFSST	Concrete-filled stainless steel tube
D	Outer diameter of the circular stainless steel tube
DI	Ductility coefficient
DS	Desalted sea sand
E_c	Elastic modulus of concrete
E_s	Elastic modulus of stainless steel
f_{ck}	Characteristic compressive strength of concrete
f_{cu}	Cubic strength of concrete
f_y	Yield strength of steel
N	Axial load
N_{ue}	Measured ultimate sectional capacity of the composite column
N_{max}	Maximum load during the loading stage
n	Strain hardening index of stainless steel
N_{uc}	Predicted ultimate sectional capacity of the composite column
RS	River sand
SI	Strength index
SS	Sea sand
t	Wall thickness of the stainless steel tube
W_{cl}	Chloride ion content
α	Steel ratio ($=A_s/A_c$)
Δ	Axial shortening of column
ε_{sl}	Longitudinal strain of the stainless steel tube
ε_{st}	Transverse strain of the stainless steel tube
$\sigma_{0.2}$	Nominal yield strength of the stainless steel tube
υ	Poisson's ratio
ξ	Confinement factor of concrete-filled steel tubes ($=\alpha \cdot f_y/f_{ck} = A_s f_y/A_c f_{ck}$)

resistance and durability, which allows untreated sea sand to be directly used [12]. In this way, sea sand concrete-filled stainless steel tube (CFSST) columns are formed, with the typical cross-sectional schematic views shown in Fig. 1.

Numerous research studies have been conducted on CFST members in terms of the mechanical properties, the numerical modelling, and the design recommendations [1–7]. Recently, the use of stainless steel has aroused the interest of researchers worldwide. It has been found that CFSST columns are feasible to be used as the main load-resisting structural elements [13–24]. Compared with traditional CFST columns, CFSST columns have better ductile behaviour and greater residual strength. Moreover, the existing design guidance for composite members with carbon steel are proved to be over-conservative when applied to CFSST members, in particular for those with circular cross-sections [15,16]. However, the vast majority of these studies focused on the common CFSST columns with traditional river sand concrete infill. Since the idea of using sea sand concrete as the core infill for CFSST columns is relatively new, it is found that only one set of experimental study has been reported, with specific focus on circular stub columns [8]. Up to date, very limited report can be found on the structural behaviour of both circular and square sea sand concrete-filled stainless steel tubular columns. The insufficient testing data and lack of evaluation on the member performance indicates a need of research in this area.

The aim of this study is to present an experimental investigation on the structural behaviour of sea sand concrete-filled stainless steel tubes. Firstly, a total of 48 CFSST specimens were prepared and tested under axial compression, among which half were with circular cross-sections while the other half with square cross-sections. Three types of core concrete, including natural river sand (RS) concrete, desalted sea sand (DS) concrete and natural sea sand (SS) concrete, were used together with stainless steel tubes in these specimens for the sake of comparison. Secondly, the structural performances of the tested CFSST specimens using these three types of core concrete were compared and analyzed based on the testing data and observation. The confinement effects provided by circular and square stainless steel tubes were also evaluated for different types of concrete. Finally, the feasibility of ultimate strength prediction for these innovative composite columns using existing design guidelines were evaluated. The structural behaviour of stub columns are focused on in the current study. The influence of important parameters are studied, including the cross-sectional shape, the steel tubular thickness, and the material properties of steel and concrete.

2. Experimental program

2.1. Specimen preparation

As stated above, a total of 48 CFSST column specimens were prepared and tested under axial compression in the present study, including 24 square members and 24 circular ones. The main parameters included the types of fine aggregates, i.e., natural river sand (RS), desalted sea sand (DS) and natural sea sand (SS), the sectional steel ratio (defined as $\alpha = A_s/A_c$ [1], where A_s is the cross-sectional area of the stainless steel tube, A_c is the cross-sectional area of the core concrete), the cross-sectional configuration and the concrete strength. Details of the test specimens are listed in Table 1, where D is the outer diameter of the circular CFSST specimens, B is the outer width of the square CFSST specimens, t is the wall thickness of the stainless steel tube, f_{cu} is the measured compressive strength of standard concrete cubic samples under the same curing condition with the CFSST specimens, ξ is the confinement coefficient taken as $A_s f_y/A_c f_{ck}$ [1], with f_y as the yield stress of the stainless steel and f_{ck} as the characteristic compressive strength of the core concrete. For circular CFSST specimens, three different tubular thicknesses (2.88, 3.80 and 4.50 mm) were designed to achieve the steel ratio α as 0.077, 0.103 and 0.124 respectively; whilst the wall thicknesses for square sections are 2.88, 3.90

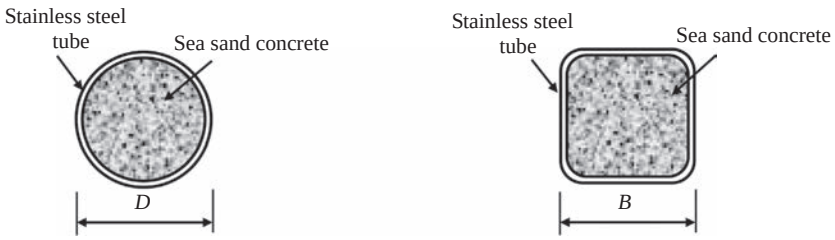

(a) Circular cross-section (b) Square cross-section

Fig. 1. Cross-sectional schematic views of sea sand CFSST columns.

Table 1
Information and the sectional capacities of the tested CFSST specimens.

Sectional profile	No.	Specimen label	D (mm)	t (mm)	Type of fine aggregates	f_{cu} (MPa)	α	$\sigma_{0.2}$ (MPa)	ξ	N_{ue} (kN)	N_{max} (kN)
Circular	1	C-3-L-RS-1	159.0	2.88	River sand (RS)	44.0	0.77	383.9	1.00	1263.6	1494.7
	2	C-3-L-RS-2	159.0	2.88		44.0	0.77	383.9	1.00	1322.2	1489.1
	3	C-3-H-RS-1	159.0	2.88		51.4	0.77	383.9	0.85	1348.7	1551.9
	4	C-3-H-RS-2	159.0	2.88		51.4	0.77	383.9	0.85	1315.6	1588.6
	5	C-4-L-RS-1	159.0	3.80		44.0	0.103	400.7	1.40	1626.8	1894.9
	6	C-4-L-RS-2	159.0	3.80		44.0	0.103	400.7	1.40	1624.0	1896.8
	7	C-5-L-RS-1	159.0	4.50		44.0	0.124	401.0	1.68	1712.9	1981.7
	8	C-5-L-RS-2	159.0	4.50		44.0	0.124	401.0	1.68	1630.1	1983.4
	9	C-3-L-DS-1	159.0	2.88	Desalted sea sand (DS)	43.3	0.77	383.9	1.01	1309.5	1528.0
	10	C-3-L-DS-2	159.0	2.88		43.3	0.77	383.9	1.01	1290.9	1540.0
	11	C-3-H-DS-1	159.0	2.88		58.7	0.77	383.9	0.75	1513.7	1686.4
	12	C-3-H-DS-2	159.0	2.88		58.7	0.77	383.9	0.75	1551.6	1603.2
	13	C-4-L-DS-1	159.0	3.80		43.3	0.103	400.7	1.42	1597.6	1780.0
	14	C-4-L-DS-2	159.0	3.80		43.3	0.103	400.7	1.42	1611.9	1900.0
	15	C-5-L-DS-1	159.0	4.50		43.3	0.124	401.0	1.71	1725.4	2080.0
	16	C-5-L-DS-2	159.0	4.50		43.3	0.124	401.0	1.71	1739.2	2115.2
	17	C-3-L-SS-1	159.0	2.88	Sea sand (SS)	42.2	0.77	383.9	1.04	1366.1	1701.2
	18	C-3-L-SS-2	159.0	2.88		42.2	0.77	383.9	1.04	1333.2	1734.6
	19	C-3-H-SS-1	159.0	2.88		52.4	0.77	383.9	0.84	1465.9	1562.5
	20	C-3-H-SS-2	159.0	2.88		52.4	0.77	383.9	0.84	1451.7	1649.3
	21	C-4-L-SS-1	159.0	3.80		42.2	0.103	400.7	1.46	1642.4	1904.3
	22	C-4-L-SS-2	159.0	3.80		42.2	0.103	400.7	1.46	1647.8	1849.0
	23	C-5-L-SS-1	159.0	4.50		42.2	0.124	401.0	1.75	1745.8	2180.9
	24	C-5-L-SS-2	159.0	4.50		42.2	0.124	401.0	1.75	1715.0	2076.6
Square	25	S-3-L-RS-1	160.0	2.88	River sand (RS)	44.0	0.76	446.2	1.15	1461.5	–
	26	S-3-L-RS-2	160.0	2.88		44.0	0.76	446.2	1.15	1534.1	–
	27	S-3-H-RS-1	160.0	2.88		51.4	0.76	446.2	0.99	1584.9	–
	28	S-3-H-RS-2	160.0	2.88		51.4	0.76	446.2	0.99	1532.8	–
	29	S-4-L-RS-1	160.0	3.90		44.0	0.105	414.5	1.48	2039.6	–
	30	S-4-L-RS-2	160.0	3.90		44.0	0.105	414.5	1.48	1930.6	–
	31	S-5-L-RS-1	160.0	4.80		44.0	0.132	431.9	1.93	2124.6	–
	32	S-5-L-RS-2	160.0	4.80		44.0	0.132	431.9	1.93	2011.9	–
	33	S-3-L-DS-1	160.0	2.88	Desalted sea sand (DS)	44.3	0.76	446.2	1.14	1543.3	–
	34	S-3-L-DS-2	160.0	2.88		44.3	0.76	446.2	1.14	1590.0	–
	35	S-3-H-DS-1	160.0	2.88		58.7	0.76	446.2	0.86	1768.8	–
	36	S-3-H-DS-2	160.0	2.88		58.7	0.76	446.2	0.86	1913.8	–
	37	S-4-L-DS-1	160.0	3.90		44.3	0.105	414.5	1.47	1955.4	–
	38	S-4-L-DS-2	160.0	3.90		44.3	0.105	414.5	1.47	1896.5	–
	39	S-5-L-DS-1	160.0	4.80		44.3	0.132	431.9	1.92	2151.5	–
	40	S-5-L-DS-2	160.0	4.80		44.3	0.132	431.9	1.92	2141.3	–
	41	S-3-L-SS-1	160.0	2.88	Sea sand (SS)	47.3	0.76	446.2	1.07	1724.6	–
	42	S-3-L-SS-2	160.0	2.88		47.3	0.76	446.2	1.07	1780.0	–
	43	S-3-H-SS-1	160.0	2.88		52.4	0.76	446.2	0.97	1689.7	–
	44	S-3-H-SS-2	160.0	2.88		52.4	0.76	446.2	0.97	1765.1	–
	45	S-4-L-SS-1	160.0	3.90		47.3	0.105	414.5	1.37	2007.7	–
	46	S-4-L-SS-2	160.0	3.90		47.3	0.105	414.5	1.37	1947.0	–
	47	S-5-L-SS-1	160.0	4.80		47.3	0.132	431.9	1.80	2215.0	–
	48	S-5-L-SS-2	160.0	4.80		47.3	0.132	431.9	1.80	2196.8	–

and 4.80 mm, creating steel ratio α of 0.076, 0.105 and 0.132 respectively. The sectional diameter D of the circular stainless steel tube is 159.0 mm, while the sectional width B of the square stainless steel tube is 160.0 mm. The height of each specimen is 480 mm, with the dimension of each endplate as 200 × 200 × 30 mm. For the labelling of specimens, the following rules apply,

- The first letter of the label represents the cross-sectional shape: 'C' for circular cross-section and 'S' for square cross-section.
- The first number of the label represents the nominal wall thickness of the stainless steel tubes: for circular specimens, '3' for 2.88 mm, '4' for 3.80 mm and '5' for 4.50 mm; for square specimens,'3' for 2.88 mm, '4' for 3.90 mm and '5' for 4.80 mm.
- The second letter of the label represents the concrete strength: for each type of specimens in this program, concrete with two levels of strength were used to prepare the specimens, as shown in Table 1. 'L' denotes the relatively lower strength concrete and 'H' the relatively higher strength concrete.
- The following two letters represents the type of fine aggregate of the core concrete: 'RS' for natural river sand, 'DS' for desalted sea sand and 'SS' for natural sea sand.
- For each set of design parameters, two CFSST members were prepared as counterparts. The last number, i.e., '1' or '2', represents the serial number of the two reference specimens.

2.2. Material properties

Grade AISI 304 austenitic stainless steel was used to fabricate the CFSST specimens. The stainless steel tubes of CFSST specimens were made in a professional fabrication workshop using cold-forming method. Before casting the concrete, the stainless steel tubes were cut into the required lengths and then a carbon steel endplate was welded to one end of each tube. In order to investigate the material properties of the stainless steel tube, stainless steel coupons were manufactured and tested in accordance with the tensile test specification GB/T228.1–2010 [25]. Particularly, for stainless steel tube with square cross-sections, coupons from the flat zones and the corner zones were tested respectively. Fig. 2(a) shows the measured typical stress (σ) - strain (ε) curves

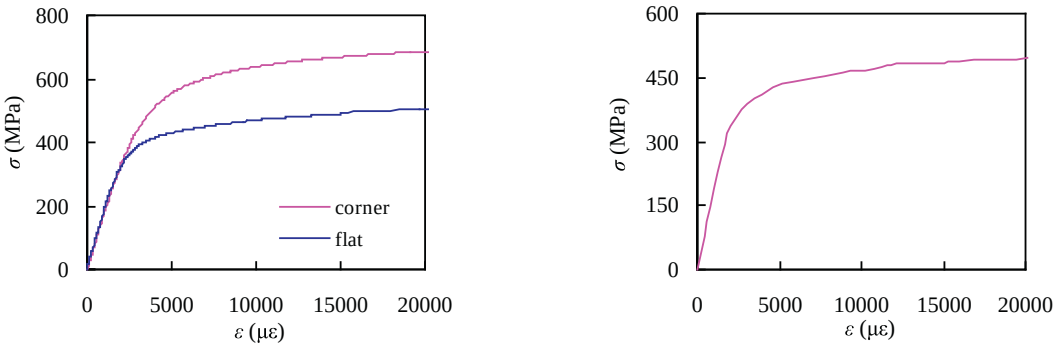

(a) Square stainless steel tube (160×3.9 mm) (b) Circular stainless steel tube (159×3.8 mm)

Fig. 2. The measured stress-strain curves of stainless steel tube used in the testing.

for square stainless steel tubes (160 × 3.90 mm), while Fig. 2(b) shows the σ-ε curve for circular stainless steel tubes (159 × 3.80 mm). It is evident that the measured σ-ε relationship showed remarkable non-linear characteristics with a significant strain hardening stage after yielding. For the square section, the yield strength of the corner steel is obviously higher than that of the flat steel, mainly due to the effect of cold-forming process. The detailed testing results for stainless steel material are listed in Table 2, in which $\sigma_{0.2}$ is the 0.2% proof stress of stainless steel, E_s is the elastic modulus of stainless steel, υ is the Poisson's ratio and n is the corresponding strain hardening index [26].

For each type of fine aggregate, self-consolidating concrete (SCC) with the designed cubic strength (f_{cu}) of 40 and 60 MPa was adopted as the core concrete of each group of CFSST specimens. The mixture proportions of the fresh concrete "cement: water: fine aggregate: coarse aggregate: fly ash: water reducing agent" were 263.7: 187.3: 759.9: 1013.3: 175.8: 4.40 (kg/m^3) for 40 MPa concrete and 260.34: 185.5: 867.8: 695.8: 390.56: 7.81 (kg/m^3) for 60 MPa concrete. Granite gravel with a maximum size of 20 mm were used as the coarse aggregates; high-efficiency water-reducing additive TW-PS was used as the water reducing agent. As mentioned before, three types of fine aggregates were used in the preparation of each mix proportion of concrete, i.e., river sand, desalted sea sand and sea sand. The photos of these three types of fine aggregates are shown in Fig. 3. Obtained from a beach in Changle District of Fuzhou City, China, the sea sand has impurities visible to naked eyes, such as shells shown in Fig. 3(c). The desalted sea sand was treated according to the Chinese Specification for sand for construction GB/T14684-2011 [27], i.e., the sea sand was immersed in fresh water for 24 h and then washed by high-pressure water gun throughout, followed by sun drying and sieving to remove visible impurities such as shells. By doing this, the salt attached to the sea sand can be partially removed, as proved by the measuring of chloride ion concentration introduced in the following paragraph. Based on the expense rate of labor and materials in Fujian province, China, a tentative analysis showed that the cost of the desalting and sieving of sea sand took up 5–10% the price of the commercial self-consolidating concrete with normal strengths. After the core concrete was poured into the stainless steel tubes in layers without any vibration, it was cured under the natural condition for 28 days. High strength epoxy mortar was then used to strengthen end gaps introduced by the natural shrinkage of concrete. This was followed by the welding of the endplate at the other column end.

Table 2
Tensile test results of the stainless steel coupons.

Sectional size D (B) × t (mm)	Cross-sectional profile	Location of the coupon	$\sigma_{0.2}$ (MPa)	υ	E_s (MPa)	n
159 × 2.88	Circular	–	383.9	0.27	195,200	3.13
159 × 3.80	Circular	–	400.7	0.26	184,433	5.07
159 × 4.50	Circular	–	401.0	0.27	177,000	7.07
160 × 2.88	Square	Flat	446.2	0.28	202,800	4.94
160 × 3.90	Square	Flat	414.5	0.27	197,400	4.63
160 × 4.80	Square	Flat	431.9	0.27	197,900	6.74
160 × 2.88	Square	Corner	556.9	0.26	191,300	3.88
160 × 3.90	Square	Corner	533.1	0.28	184,300	5.48
160 × 4.80	Square	Corner	543.9	0.29	182,000	5.00

The content of chloride ion (W_{cl}) in the sand was measured using the method of silver nitrate titration in accordance with the above mentioned GB/T14684-2001 on sand for construction [27] and the Chinese Construction Industry Specification for sand testing JGJ52-2006 [28]. The sand sample was immersed and agitated in distilled water so that the chloride ion was dissolved. A process of filtration and titration using chromate indicator and silver nitrate solution was then conducted to determine the chloride ion concentration of the solution produced by the immersed sand. The average value of three measure trials for each set of sand samples was determined and shown in Table 3. The test results showed that the chloride ion content W_{cl} of sea sand was the highest (0.14%), and those of the desalted sea sand and the river sand were 0.06% and 0.006%, respectively. The measured material properties of the concrete, such as the cubic compressive strength (f_{cu}), the elastic modulus (E_c), the slumps and slump flows are listed in Table 3 as well. It was found that, in general, the mechanical property and workability of sea sand concrete is close to those of the river sand concrete and desalted sea sand concrete, except that the slump and slump flow of sea sand concrete are slightly lower. It should be noted that, for CFSST specimens filled with desalted sea sand and sea sand concrete, square column specimens were tested one month later than the circular ones due to lab schedule. As a result, the strengths of desalted sea sand concrete and sea sand concrete developed to 44.3 and 47.3 MPa respectively when the square CFSST specimens were tested.

2.3. Test setup

The tests were conducted using a 5000 kN compressive testing machine. The test setup is illustrated in Fig. 4. Prior to the applying of the axial compressive load, the specimens were strictly centered and preloaded to eliminate potential gaps in the test setup. The tests were conducted under multi-stage loading, with each loading step of about a tenth of the estimated sectional bearing capacity at the initial loading stage. When the estimated ultimate load was approached, continuous displacement loading with a slow speed was applied on the specimen to obtain its softening response, with the loading rate of appropriately 0.005 mm/s. A specimen was considered being failure when the load decreased to 75% of its ultimate sectional bearing capacity, the loading procedure would then be terminated. For specimens without obvious descending stage, the loading is terminated when the axial displacement reached around 1/10 of the height of the specimen. In order to record the development of the strain of stainless steel tubes during the

(a) River sand (b) Desalted sea sand (c) Sea sand

Fig. 3. Three types of fine aggregates used in the testing.

loading process, eight strain gauges were attached at the mid-height cross section, including one vertically positioned longitudinal gauge and one horizontally positioned circumferential gauge for each measuring point, as shown in Fig. 4. In addition, four high-accuracy linear variable displacement transducers (LVDTs) were arranged to measure the axial shortening of the tested CFSST specimens.

3. Experimental results

3.1. Typical failure modes of the tested CFSST specimens

The failure patterns of the circular and square CFSST specimens after testing are displayed in Figs. 5(a) and (b) respectively. As shown in Fig. 5, most of the circular CFSST specimens had obvious local buckling at the mid-height of the tube, whilst the square CFSST specimens tended to buckle in wave pattern. Such differences were consistent with the previously reported studies on different confining effects in CFST with the two types of sectional shapes [1]. The stainless steel exhibited very good deformation ability, where no fracture was observed for most of the tested specimens even under severe buckling conditions. The failure modes of all CFSST specimens were outward buckling instead of inward buckling due to the inner support provided by the core concrete. During the loading process, it was observed that the local buckling of stainless steel tended to occur earlier for CFSST specimen with a lower steel ratio. The influence of concrete prepared with three different types of fine aggregates on the failure modes of typical circular and square CFSST specimens are compared in Figs. 6(a) and (b). It is clear that the variation of fine aggregates has only moderate effects on the failure mode of CFSST columns.

Fig. 7 shows the exposed failure mode of the sea sand concrete in CFSST columns after testing. It can be seen that the interface of the stainless steel tubes and three types of core concrete remained intact after the testing. Due to the confinement effect of the stainless steel tube, no overall crack was observed along the core concrete, whilst obvious local crushing could be seen at positions where the stainless steel tube buckled. Compared with the square CFSST specimens, less significant crushing of the sea sand concrete was shown in circular CFSST since the circular stainless steel tube could provide stronger confinement than the square counterpart. In general, the failure pattern of the sea sand concrete is very similar with that of the conventional river sand concrete in a CFSST stub column.

Table 3
Material test results of the core concrete.

Type of fine aggregates	W_{cl} (%)	f_{cu} (MPa)	E_c (MPa)	Slump (mm)	Slump flow (mm)
River sand	0.006	44.0	29,405.9	240	630
		51.4	30,350.1	280	730–740
Desalted sea sand	0.06	43.3(circular)/ 44.3(square)	30,795.9	230	620–640
		58.7	31,838.2	280	720–760
Sea sand	0.14	42.2(circular)/ 47.3(square)	28,441.2	220	430–520
		52.4	31,009.8	250	550–600

3.2. Axial load (N) versus axial shortening (Δ) relations of the tested CFSST specimens

Fig. 8(a) and (b) show the measured load (N) – axial shortening (Δ) relations of all the circular and square CFSST specimens, respectively. With either conventional river sand concrete or sea sand concrete infill, the tested CFSST specimens showed considerably ductile behaviour without sudden drop of load. It is clear that the load-shortening curves exhibited elastic pattern during the initial loading stage. Then after the stainless steel tube yielded and the elastic-plastic stage was reached, the stiffness of the curves tend to decrease with the increasing load and the curves started to show non-linear features.

As can be seen in Fig. 8(a), there was no descending stage at the N-Δ curves for circular CFSST specimens. This again attributed to the strong confinement effect provided by the circular stainless steel tube on the sea sand concrete, as well as the significant strain hardening of stainless steel tube. As a result, circular CFSST specimens had better ductility, with their N-Δ curves increasing slowly until the end of the loading, even after the axial deformation was considerably large. With the increasing of the steel tubular thickness, the hardening effects at the later stage became more obvious. The N-Δ curves of the circular CFSST specimens in this paper can be approximately classified as “Type A” curve based on the research by [15].

The N-Δ curves of the square CFSST specimens also experienced elastic stage and then elastic-plastic stage. After that, there was visible local buckling of stainless steel tube when the ultimate sectional capacity was approached. Compared with the circular one, square stainless steel tubes provided less confinement effects on the core concrete. As a result, gradually decreasing stage of the N-Δ curves were observed after the ultimate sectional capacity was reached. The N-Δ curves of the square CFSST specimens in this paper can be classified as “Type C” curve based on the research by [15]. Overall, CFSST specimens had excellent deformation capacity due to the high elongation rates and the significant strain hardening effects of stainless steel material.

Fig. 9 compares the N-Δ curves of the tested CFSST specimens to evaluate the influence of different sets of parameters. It is clear that the three types of fine aggregates had only moderate influence on the N-Δ curves. With other parameters being the same, the shape of N-Δ curves for CFSST with sea sand concrete is generally in accordance with that of CFSST with conventional river sand concrete, as shown in Figs. 9(a1 and a2). This proves that the confinement effects of stainless steel tube could greatly eliminate the unfavorable effects brought by the impurities of sea sand such as chloride iron and shells. With the increase of concrete strength, the N-Δ curves of square CFSST specimens had greater ultimate sectional strength however experienced steeper decreasing tendency and less ductility, as displayed in Fig. 9(b2). With the increase of the stainless steel tubular thickness, the N-Δ curves of circular CFSST specimens showed more obvious upward tendency at the late stage as shown in Fig. 9(a1), while the N-Δ curves of the square ones descended more gently as shown in Fig. 9(a2), illustrating

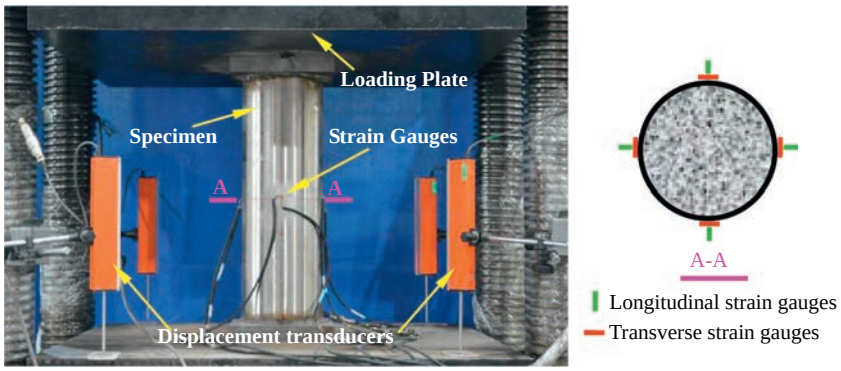

Fig. 4. Photo of the test set up.

enhanced ductility and deformation capacity. This was consistent with the observation for CFST columns in [1,15], which can be explained using the above described confinement factor ξ. The confinement factor ξ is defined to quantitatively describe the confinement effect of the steel tube on its core concrete, i.e., the larger ξ is, the stronger the confinement effect. As indicated, the increase of the thickness of steel tube could lead to the increase of ξ, indicating better material confinement and thus enhanced ductility in CFSST columns.

3.3. Axial load (N) versus strain (ε) relations of the tested CFSST specimens

Fig. 10 shows the axial load (N) versus longitudinal strain (ε_{sl}) and transverse strain (ε_{st}) relations of the tested CFSST specimens, where the longitudinal strain was plotted at the positive side and the transverse strain was plotted at the negative side. The strain corresponding to the nominal yield strength of the stainless steel tube $\sigma_{0.2}$, i.e., ε_{sy}, has been marked in Fig. 10. In each figure, the strain developments of stainless steel tubes were compared when the fine aggregates of the core concrete varied whilst all other factors remaining the same. To some extent, the transverse strain of the steel tube can reflect the development of the composite action between the stainless steel tube and the core concrete. During the elastic stage, transverse strain with very small values were developed in the steel tubes initially. At this time, no contact between the steel tube and the core concrete was generated, therefore the transverse strain was only about 30% of the longitudinal strain, i.e., basically caused by the Poisson's ratio of the stainless steel. Afterwards, with the increase of the axial load, contact between the stainless steel and the core concrete was developed due to the lateral expansion of concrete under high stress level. As a result, rapid development of the transverse stain was seen for the stainless steel tube, while the core concrete started to get confined by the stainless steel tube at the meantime. Particularly, after the stainless steel tube reached its nominal yield strength, its transverse strain developed at an even faster speed along with the cracking of the core concrete. For circular CFSST specimens, the development of transverse strain kept growing rapidly until the end of the loading, illustrating effective confinement effects of steel tube during the whole loading stage, as shown in Fig. 10(a). For square CFSST specimens, the ultimate sectional capacity was reached once the steel tube reached its nominal yield strength. After that, the transverse strain of the stainless steel tube developed rapidly while the applied compressive load gradually decreased, as shown in Fig. 10(b).

In general, the influence of the three types of fine aggregates on the strain of stainless steel tube was insignificant. The transverse strain of CFSST specimens with sea sand concrete or desalted sea sand concrete developed rapidly after its core concrete contacting to the steel tube, indicating effective confinement provided by the stainless steel tube for sea sand concrete during the loading process.

4. Analysis and discussion

4.1. Ultimate sectional capacity

Figs. 11 (a) and (b) compare the ultimate sectional capacity (N_{ue}) of the tested circular and square CFSST specimens respectively. It should be noted that since there is normally no obvious descending stage in

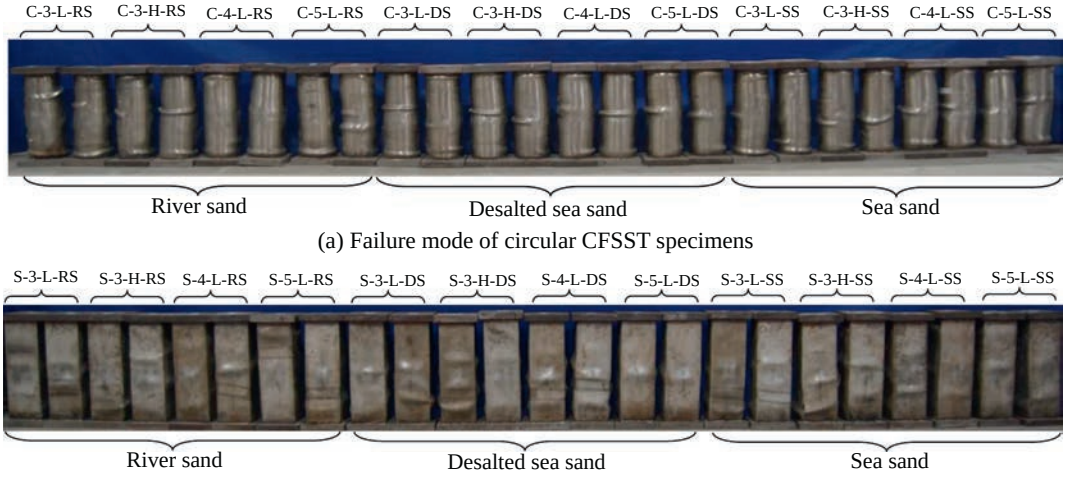

(a) Failure mode of circular CFSST specimens

(b) Failure mode of square CFSST specimens

Fig. 5. Failure mode of the tested specimens.

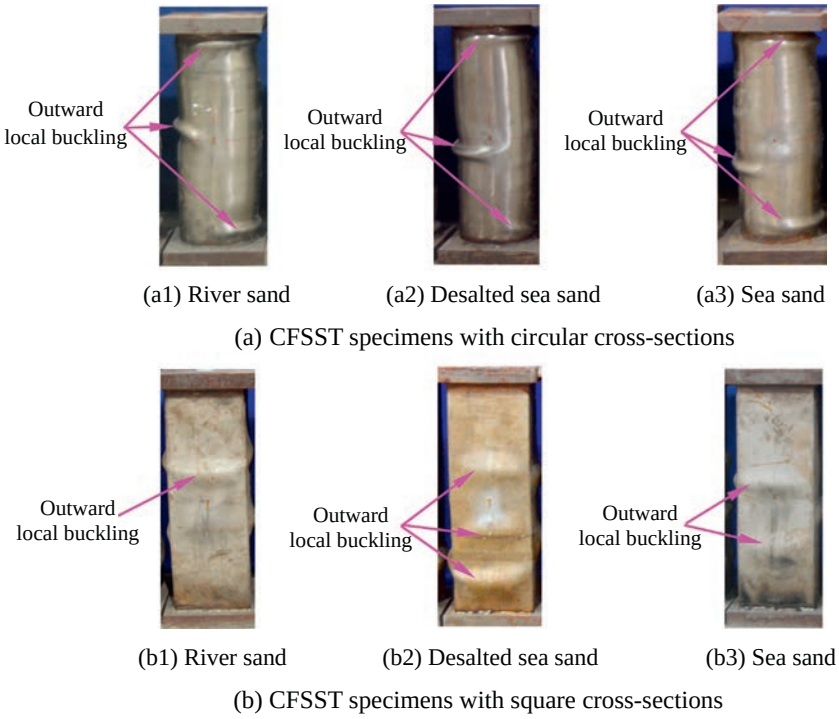

Fig. 6. Comparison of the failure modes for specimens prepared with different types of fine aggregates.

the N-Δ curves of circular CFSST specimens, the ultimate sectional capacity N_{ue} is taken as the axial load value corresponding to an axial strain limit of 10,000 με [15]. The ultimate sectional capacity N_{ue} of a square CFSST specimen is taken as the direct peak value from its N-Δ curve. As can be seen from Fig. 11, the types of fine aggregates have no significant influence on the variation tendency of the ultimate

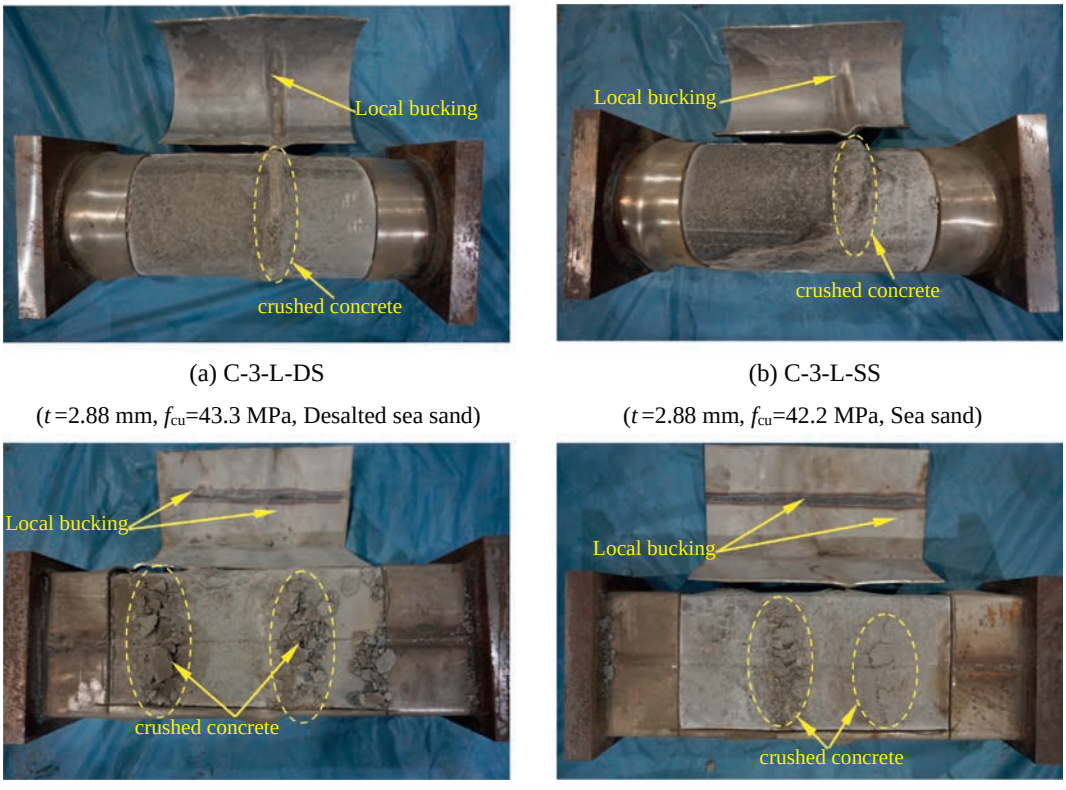

Fig. 7. Exposed view of the core concrete in CFSST specimens after testing.

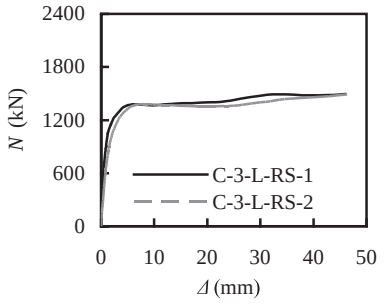

(a1) C-3-L-RS
(t =2.88 mm, f_{cu}=44.0 MPa, River sand)

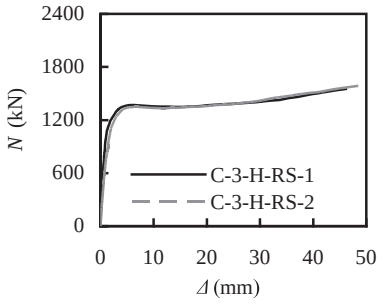

(a2) C-3-H-RS
(t =2.88 mm, f_{cu}=51.4 MPa, River sand)

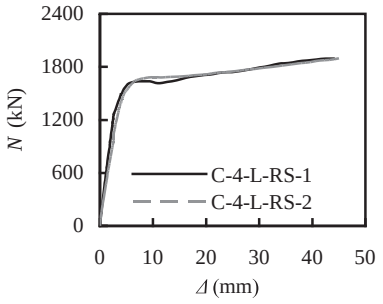

(a3) C-4-L-RS
(t =3.90 mm, f_{cu}=44.0 MPa, River sand)

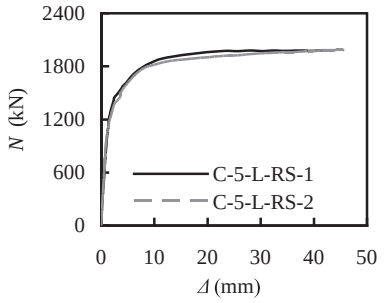

(a4) C-5-L-RS
(t =4.50 mm, f_{cu}=44.0 MPa, River sand)

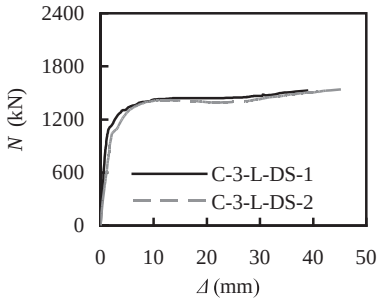

(a5) C-3-L-DS
(t =2.88 mm, f_{cu}=43.3 MPa, Desalted sea sand)

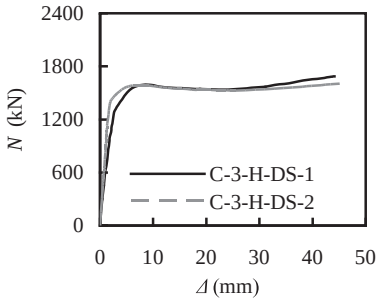

(a6) C-3-H-DS
(t =2.88 mm, f_{cu}=58.7 MPa, Desalted sea sand)

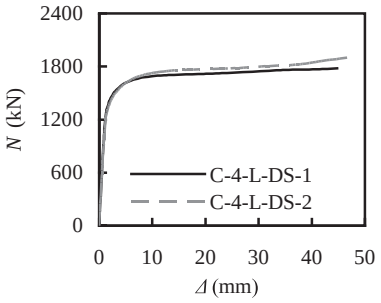

(a7) C-4-L-DS
(t =3.90 mm, f_{cu}=43.3 MPa, Desalted sea sand)

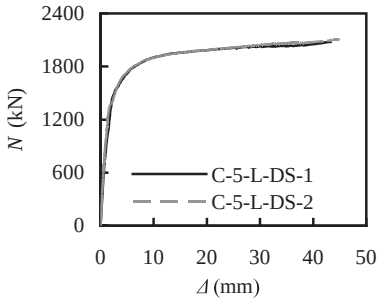

(a8) C-5-L-DS
(t =4.50 mm, f_{cu}=43.3 MPa, Desalted sea sand)

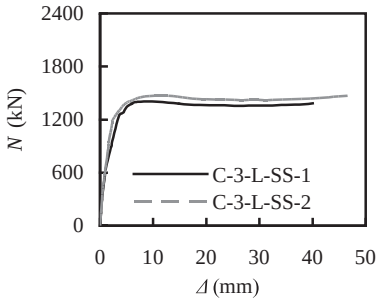

(a9) C-3-L-SS
(t =2.88 mm, f_{cu}=42.2 MPa, Sea sand)

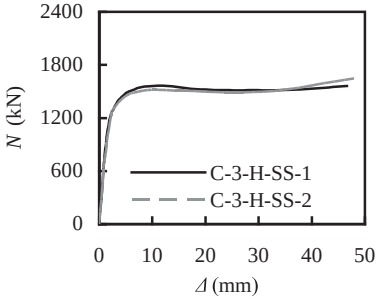

(a10) C-3-H-SS
(t =2.88 mm, f_{cu}=52.4 MPa, Sea sand)

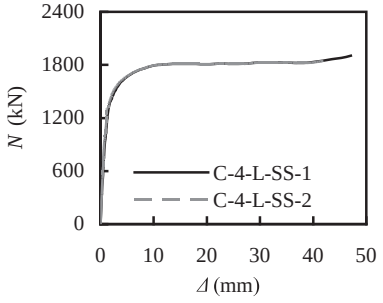

(a11) C-4-L-SS
(t =3.90 mm, f_{cu}=42.2 MPa, Sea sand)

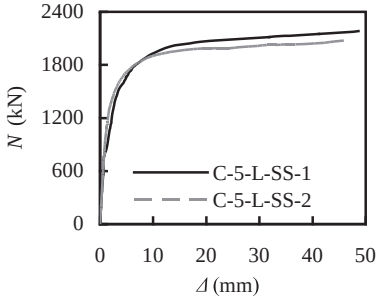

(a12) C-5-L-SS
(t =4.50 mm, f_{cu}=42.2 MPa, Sea sand)

(a) CFSST specimens with circular cross-sections

Fig. 8. Axial load (N) - axial shortening (Δ) relations of the tested CFSST specimens

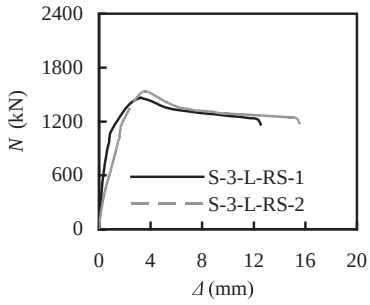

(b1) S-3-L-R
(t =2.88 mm, f_{cu}=44.0 MPa, River sand)

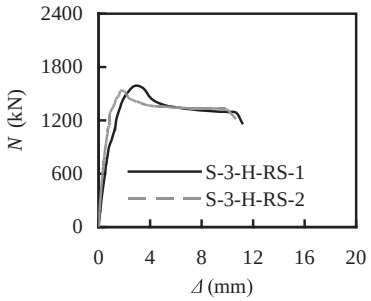

(b2) S-3-H-RS
(t =2.88 mm, f_{cu}=51.4 MPa, River sand)

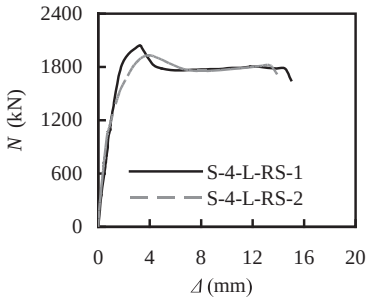

(b3) S-4-L-RS
(t =3.90 mm, f_{cu}=44.0 MPa, River sand)

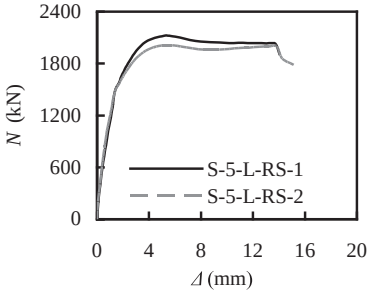

(b4) S-5-L-RS
(t =4.80 mm, f_{cu}=44.0 MPa, River sand)

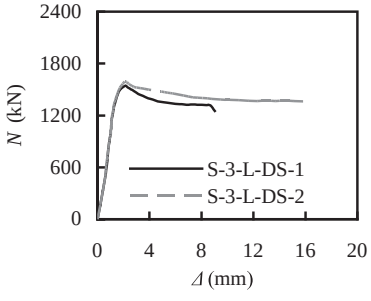

(b5) S-3-L-DS
(t =2.88 mm, f_{cu}=44.3 MPa, Desalted sea sand)

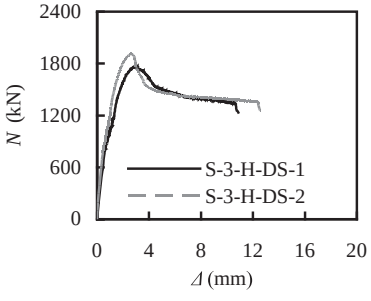

(b6) S-3-H-DS
(t =2.88 mm, f_{cu}=58.7 MPa, Desalted sea sand)

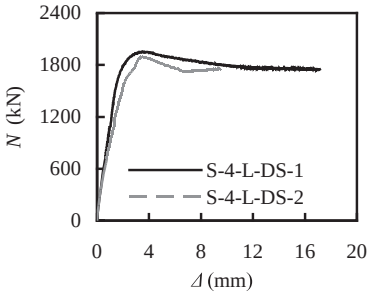

(b7) S-4-L-DS
(t =3.90 mm, f_{cu}=44.3 MPa, Desalted sea sand)

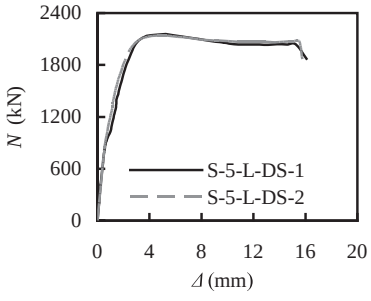

(b8) S-5-L-DS
(t=4.80 mm, f_{cu}=44.3 MPa, Desalted sea sand)

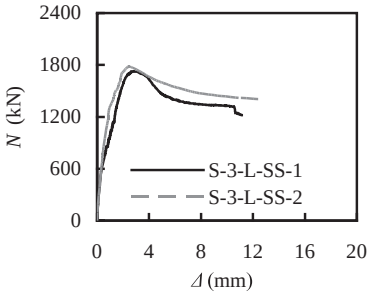

(b9) S-3-L-SS
(t =2.88 mm, f_{cu}=47.3 MPa, Sea sand)

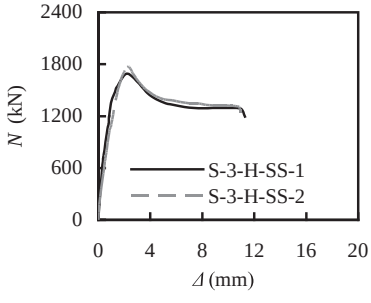

(j) S-3-H-SS
(t =2.88 mm, f_{cu}=52.4 MPa, Sea sand)

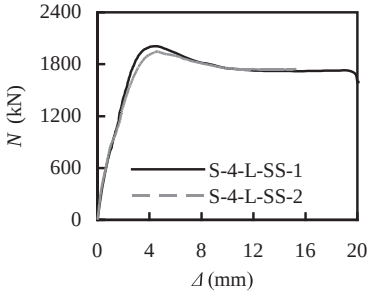

(k) S-4-L-SS
(t =3.90 mm, f_{cu}=47.3 MPa, Sea sand)

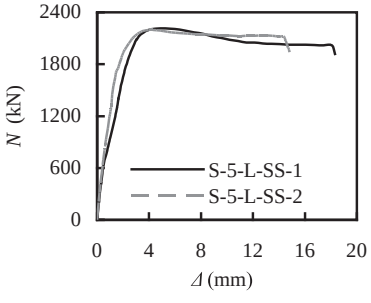

(l) S-5-L-SS
(t =4.50 mm, f_{cu}=47.3 MPa, Sea sand)

(b) CFSST specimens with square cross-sections

Fig. 8 (*continued*).

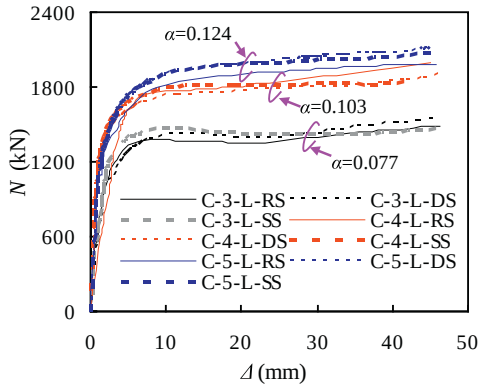

(a1) Circular section

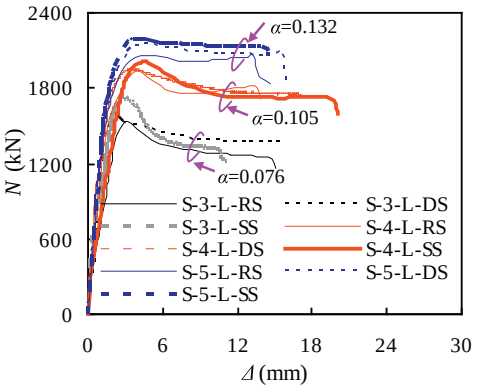

(a2) Square section

(a) Effects of different types of fine aggregates

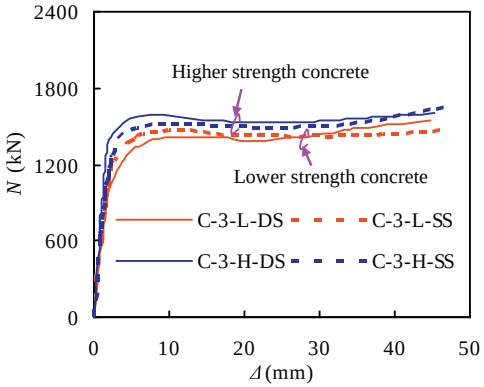

(b1) Circular section

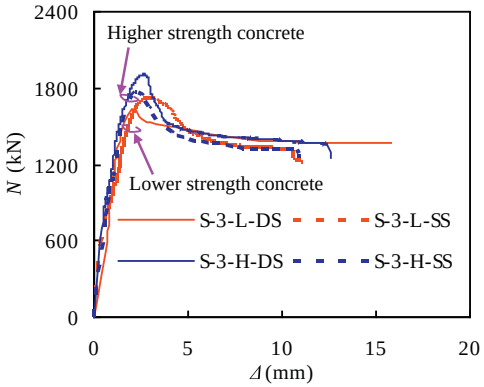

(b2) Square section

(b) Effects of the concrete strength

Fig. 9. Comparison of the *N*-Δ curves of CFSST specimens with different parameter series.

sectional capacity of CFSST columns. This attributes to the fact that, when only short-term loading is considered, the effects of the unfavorable properties of sea sand concrete on the sectional capacity is very limited as long as the concrete strength is comparable and the confinement is effective. Although it can be expected that, when it comes to long-term loading conditions, the sea sand concrete might cause issues due to its potentially unique shrinkage and creep phenomenon as well as durability risks.

As shown in Fig. 11, the ultimate sectional capacities of all CFSST specimens increase when the steel tube becomes thicker which results in larger steel ratios and stronger confinement effects. For circular CFSST specimens, when the steel ratio α increases from 0.077 to 0.124, the ultimate sectional capacity N_{ue} increases by 29.2%, 33.2% and 28.2% for core concrete made from river sand, desalted sea sand and sea sand, respectively. For square CFSST specimens, when α increases from 0.076 to 0.132, N_{ue} increases by 38.0%, 37.0% and 25.8% for core concrete made from river sand, desalted sea sand and sea sand, respectively. Meanwhile, with the same tubular thickness of stainless steel, the ultimate sectional capacities N_{ue} of CFSST specimens increase when the concrete strength increases. It is notable from Fig. 11 that, regardless the different types of core concrete in CFSST columns, the main factor affecting the ultimate sectional capacities of the specimens is the strength of the core concrete. For example, for square CFSST specimens with similar steel ratio α around 0.076 shown in Fig. 11(b), the concrete strength of river sand concrete, desalted sea sand concrete and sea sand concrete were 44.0, 44.3 and 47.3 MPa, respectively. As a result, the ultimate sectional capacities of CFSST columns with desalted sea sand concrete infill and sea sand concrete infill were 4.6% and 17.0% higher than that of the CFSST with river sand concrete infill.

In order to quantitatively evaluate the confinement effects in CFSST columns with sea sand concrete infill and conventional concrete infill, a strength index$SI_1$is defined as follows:

$$SI_1 = N_u/N_0 \tag{1}$$

Where N_u is the ultimate sectional capacity of a CFSST specimen obtained from the tests (the average value of two specimens with the same set of parameters); N_0 is the mathematical summation of the compressive strength of the stainless steel tube section and the core concrete section, i.e., $N_0 = A_c f_{ck} + A_s \sigma_{0.2}$, where A_c and A_s are the cross-sectional areas of concrete and stainless steel tube respectively; f_{ck} is the characteristic compressive strength of concrete and $\sigma_{0.2}$ is the nominal yield strength of the stainless steel tube. To some extent, SI_1 can reflect the confinement effects of the stainless steel tube on its core concrete in terms of the compressive strength of the composite cross-section.

Fig. 12 compares the variation of SI_1 with changing diameter-thickness ratio (D/t) for circular CFSST specimens and width-thickness ratio (B/t) for square CFSST specimens. Through comparison of the curves in Figs. 12(a) and (b), it can be easily concluded that the confinement effects provided by a circular stainless steel tube are greater than that by a square one. SI_1 of the evaluated circular CFSST specimens are

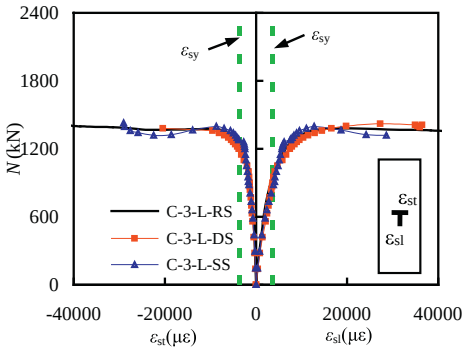

(a1) α = 0.077, Concrete with lower strength

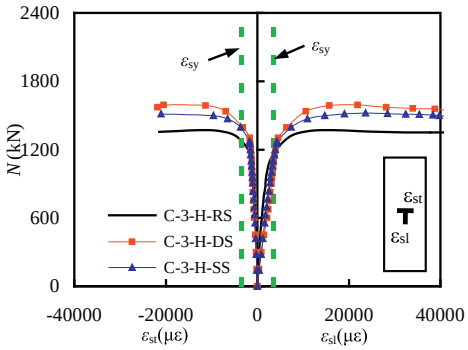

(a2) α = 0.077, Concrete with higher strength

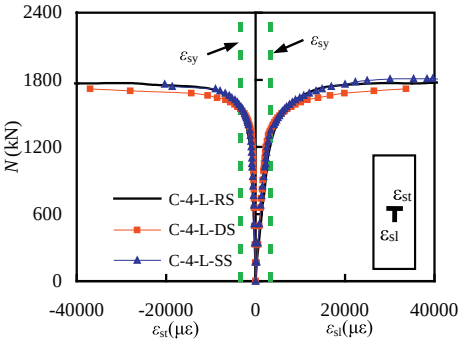

(a3) α = 0.103

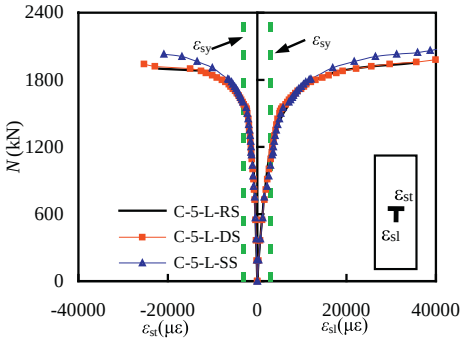

(a4) α = 0.124

(a) CFSST specimens with circular cross-sections

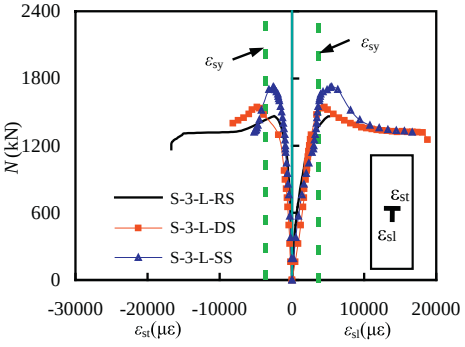

(b1) α = 0.076, Concrete with lower strength

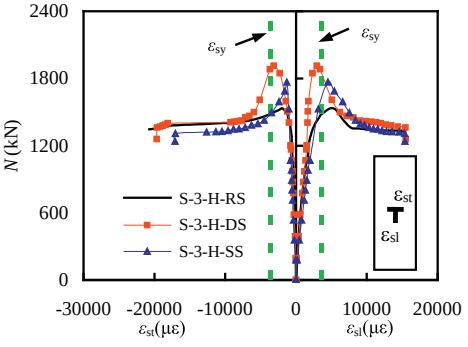

(b2) α = 0.076, Concrete with higher strength

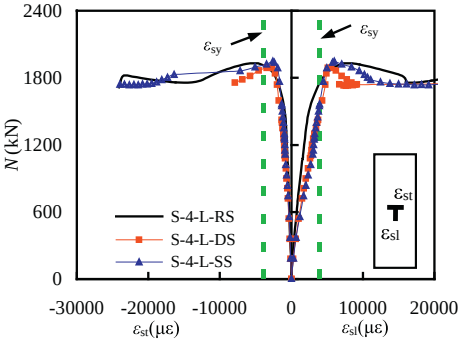

(b3) α = 0.105

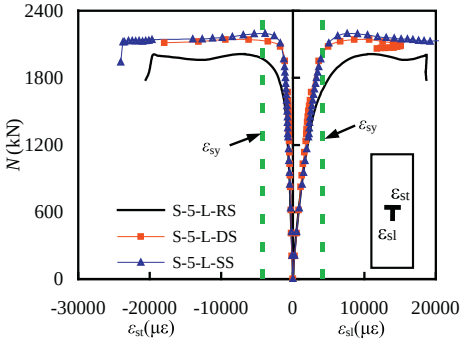

(b4) α = 0.132

(b) CFSST specimens with square cross-sections

Fig. 10. Axial load (N) - strain (ε) relations of the tested CFSST specimens.

all greater than 1.2, indicating that the ultimate sectional capacity of CFSST is increased by over 20% than the simple summation of the stainless steel tube capacity and the core concrete capacity due to the confinement effects. However, SI_1 of the evaluated square CFSST specimens are allocated from 1.0 to 1.17. Specifically, when the width-thickness ratio B/t = 56, the ultimate sectional capacity of river sand

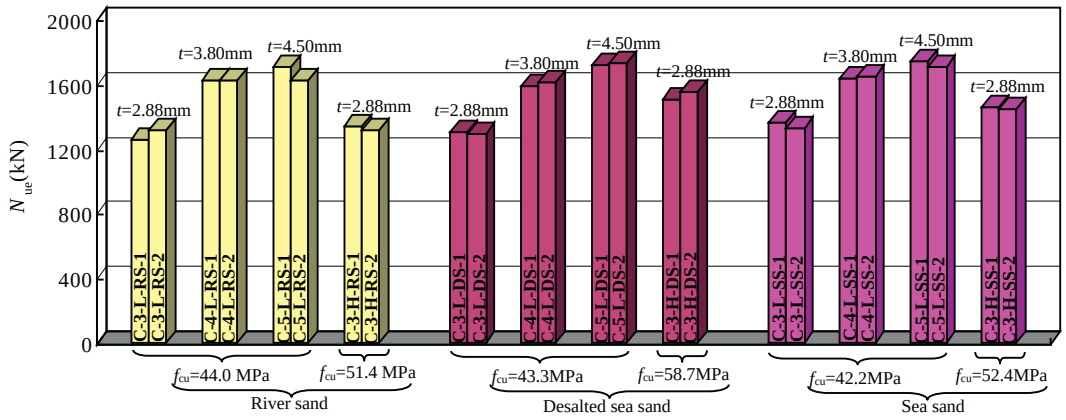

(a) CFSST specimens with circular cross-sections

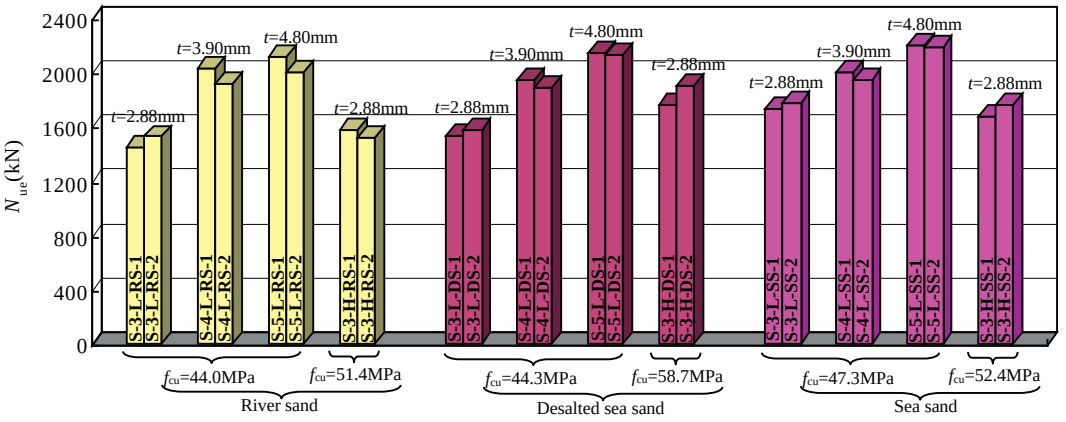

(b) CFSST specimens with square cross-sections

Fig. 11. Comparison of the ultimate sectional capacity of the tested CFSST specimens.

CFSST are generally not improved compared to the summation of its individual steel and concrete parts. This indicates that when the B/t ratio is large, the confinement effect provided by the stainless steel tube can be considerably limited.

As shown in Figs. 12(a) and (b), the differences in SI_1 values of CFSST specimens with three types of core concrete tend to be reduced with the decrease of diameter-thickness ratio (D/t) or width-thickness ratio (B/t). This can be explained by the fact that the decrease of D/t or B/t indicates increased cross-sectional steel ratio α and confinement factor ξ. With the enhanced confinement effects of stainless steel tube, the differences caused by the three types of fine aggregates can be minimized. According to the above discussions on Fig. 12, it can be concluded that the confinement effects of stainless steel on sea sand concrete is as reliable as that on conventional river sand concrete. To further validate this, another factor$SI_2$is defined as follows:

$$SI_2 = SI_1/SI_{1-RS} \tag{2}$$

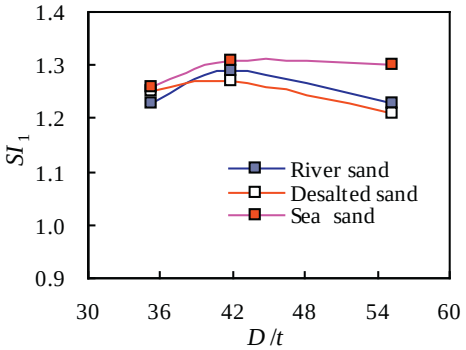

(a) SI_1 for circular CFSST specimens

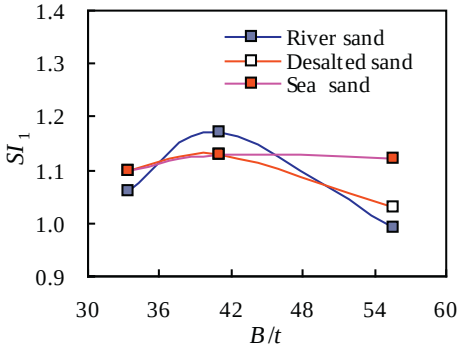

(b) SI_1 for square CFSST specimens

Fig. 12. Strength index (SI_1) of the tested CFSST specimens.

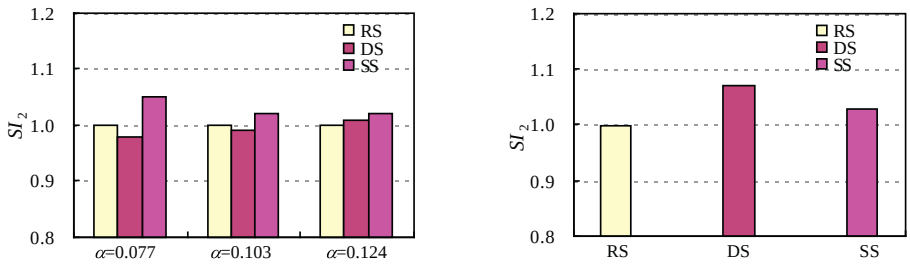

(a1) Concrete with lower strength (a2) Concrete with higher strength

(a) SI_2 for circular CFSST specimens

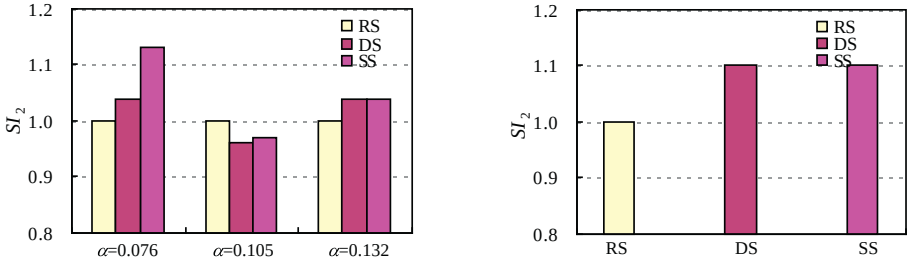

(b1) Concrete with lower strength (b2) Concrete with higher strength

(b) SI_2 for square CFSST specimens

Fig. 13. Comparison of the sectional capacity coefficient SI_2 for the tested CFSST specimens.

Where SI_1 is the strength index calculated using Eq.1, while $SI_{1\text{-RS}}$ is the specific strength index of the reference CFSST with river sand as fine aggregate.

The values of SI_2 for selected CFSST members with circular and square cross-sections are compared in Fig. 13. It can be seen that, within the range of parameters in this testing program, SI_2 of CFSST with desalted sea sand concrete and sea sand concrete are greater than 1 under most circumstances for both circular and square specimens. For example, the average values of SI_2 of circular CFSST specimens with desalted sand concrete and sea sand concrete are 1.00 and 1.04 respectively, and those of square ones are 1.04 and 1.06 respectively. This again proves that the confinement effects of stainless steel tube on sea sand concrete is as reliable as that on the conventional concrete. The usage of sea sand concrete replacing conventional concrete would not introduce significant influence on the ultimate sectional capacity of CFSST columns. This owes to the fact that the confinement of stainless steel tube on core concrete tends to reduce the potential drawbacks of the sea sand concrete.

4.2. Ductility

For the sake of quantitatively comparing the influences of various factors on the ductility of the tested CFSST specimens, a ductility coefficient (DI) defined in [29] is adopted as following:

$$DI = \varepsilon_{85\%}/\varepsilon_y \tag{3}$$

Where $\varepsilon_{85\%}$ is the average longitudinal strain of the stainless steel tube when the applied load decreases to 85% of the ultimate sectional capacity; $\varepsilon_y = \varepsilon_{75\%}/0.75$ and $\varepsilon_{75\%}$ is the average longitudinal strain of the stainless steel tube when the applied load reaches 75% of the ultimate sectional capacity in the ascent stage. The DI value for CFSST specimen with a certain set of parameters is determined by the average value of the tested two specimens in this set. As discussed before, it is notable from Figs. 8 and 9 that circular CFSST specimens generally have excellent ductility, with no descending stages in their N-Δ curves. Therefore, only the DI values of square CFSST specimens were obtained and evaluated.

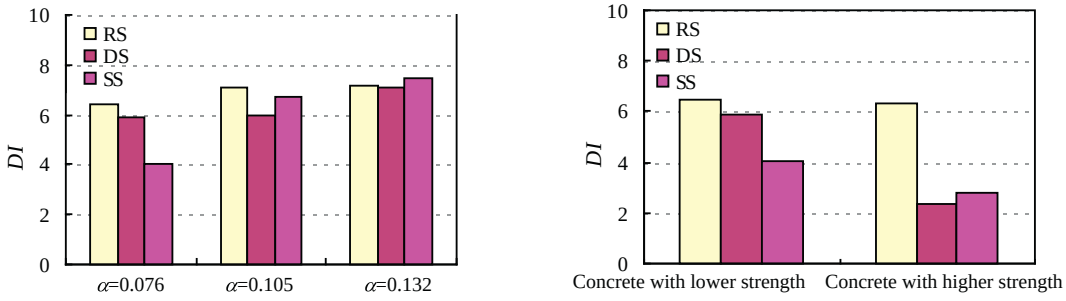

(a) Effects of steel ratio (b) Effects of concrete strength

Fig. 14. Comparison of the ductility for square CFSST specimens.

Table 4
Comparisons between the measured and predicted ultimate sectional capacity of circular CFSSTs.

Specimen label	N_{ue} (kN)	DBJ/T13-51-2010 (2010)		EC4 (2004)		ANSI/AISC 360–10 (2010)	
		N_{DBJ} (kN)	N_{ue}/N_{DBJ}	N_{EC4} (kN)	N_{ue}/N_{EC4}	N_{ASIC} (kN)	N_{ue}/N_{ASIC}
C-3-L-RS-1	1263.6	1252.8	1.01	1325.9	0.95	1139.0	1.11
C-3-L-RS-2	1322.2	1252.8	1.06	1325.9	1.00	1139.0	1.16
C-3-H-RS-1	1348.7	1344.7	1.00	1395.1	0.97	1239.4	1.09
C-3-H-RS-2	1315.6	1344.7	0.98	1395.1	0.94	1239.4	1.06
C-4-L-RS-1	1807.6	1491.6	1.21	1589.1	1.14	1323.2	1.37
C-4-L-RS-2	1644.0	1491.6	1.10	1589.1	1.03	1323.2	1.24
C-5-L-RS-1	1712.9	1660.2	1.03	1759.5	0.97	1444.7	1.19
C-5-L-RS-2	1630.1	1660.2	0.98	1759.5	0.93	1444.7	1.13
C-3-L-DS-1	1309.5	1244.0	1.05	1319.3	0.99	1129.5	1.16
C-3-L-DS-2	1290.9	1244.0	1.04	1319.3	0.98	1129.5	1.14
C-3-H-DS-1	1513.7	1430.1	1.06	1459.6	1.04	1338.3	1.13
C-3-H-DS-2	1551.6	1430.0	1.09	1459.6	1.06	1338.3	1.16
C-4-L-DS-1	1597.6	1480.4	1.08	1584.2	1.01	1313.9	1.22
C-4-L-DS-2	1611.9	1480.4	1.09	1584.2	1.02	1313.9	1.23
C-5-L-DS-1	1725.4	1653.4	1.04	1754.7	0.98	1435.6	1.20
C-5-L-DS-2	1739.2	1653.4	1.05	1754.7	0.99	1435.6	1.21
C-3-L-SS-1	1366.1	1229.7	1.11	1308.6	1.04	1114.6	1.23
C-3-L-SS-2	1333.2	1229.7	1.08	1308.6	1.02	1114.6	1.20
C-3-H-SS-1	1465.9	1356.7	1.08	1404.2	1.04	1252.9	1.17
C-3-H-SS-2	1451.7	1356.7	1.07	1404.2	1.03	1252.9	1.16
C-4-L-SS-1	1642.4	1469.0	1.12	1572.7	1.04	1299.3	1.26
C-4-L-SS-2	1647.8	1469.0	1.12	1572.7	1.05	1299.3	1.27
C-5-L-SS-1	1745.8	1637.6	1.07	1743.5	1.00	1421.2	1.23
C-5-L-SS-2	1715.0	1637.6	1.05	1743.5	0.98	1421.2	1.21
Mean		1.07		1.01		1.19	
Standard deviation		0.05		0.05		0.07	

Comparison of the ductility coefficient *DI* of the tested square CFSST specimens are shown in Fig. 14. It can be seen that *DI* increases with the increase of steel ratio, whilst it decreases with the increase of the concrete strength. This can be explained that both the increase of steel ratio α and the decrease of concrete strength f_{ck} would lead to a larger confinement factor ξ, i.e., the enhancement of confinement effect on the core concrete. In general, *DI* of the CFSST with sea sand concrete is less than that of the CFSST counterpart with river sand concrete, with narrowed gap if the steel ratio increases or the concrete strength decreases. For example, when steel ratio $\alpha = 0.076$, *DI* of CFSST with river sand concrete is 7.45, whilst *DI* of CFSST with desalted sea sand concrete and sea sand concrete are 5.90 (decreased by 8.5%) and 4.06 (decreased by 31.3%), respectively. However, when steel ratio α increased to 0.132, *DI* of CFSST with river sand concrete, desalted sea sand concrete and sea sand concrete are 7.17, 7.10 and 7.47 respectively, with minor differences observed. This proves that stronger confinement effect provided by the stainless steel tube can bring effective benefits to reduce the disadvantages of sea sand concrete.

5. Strength prediction of sea sand CFSST members

Currently, design regulations of traditional CFST columns can be found in several existing codes of practice worldwide. However, there has not been any regulation specialized in concrete-filled stainless steel tube or sea sand concrete-filled steel tube yet. In order to investigate the applicability of existing design guidelines in predicting the sectional capacity of sea sand CFSST columns under axial compression, the measured ultimate sectional capacity of sea sand CFSST specimens are predicted in accordance with existing design regulations for carbon steel CFST with conventional river sand concrete. In this section, three commonly adopted design standards, including the U.S. specification AISC-360-10 (2010) [30], Chinese local code DBJ/T13-51-2010 (2010) [31], Eurocode EC4 (2004) [32] are employed to calculate the ultimate sectional capacity of the tested CFSST specimens. To ensure the compatibility of the calculation results, the material partial safety factors are all set to unity.

For circular CFSST specimens, the calculated ultimate sectional capacities (N_{uc}) are listed and compared with those measured in this testing program (N_{ue}) in Table 4. Fig. 15 compares the ratios between the measured and the predicted results (N_{ue}/N_{uc}) against different confinement coefficient ξ. It can be seen that, for circular CFSST, the

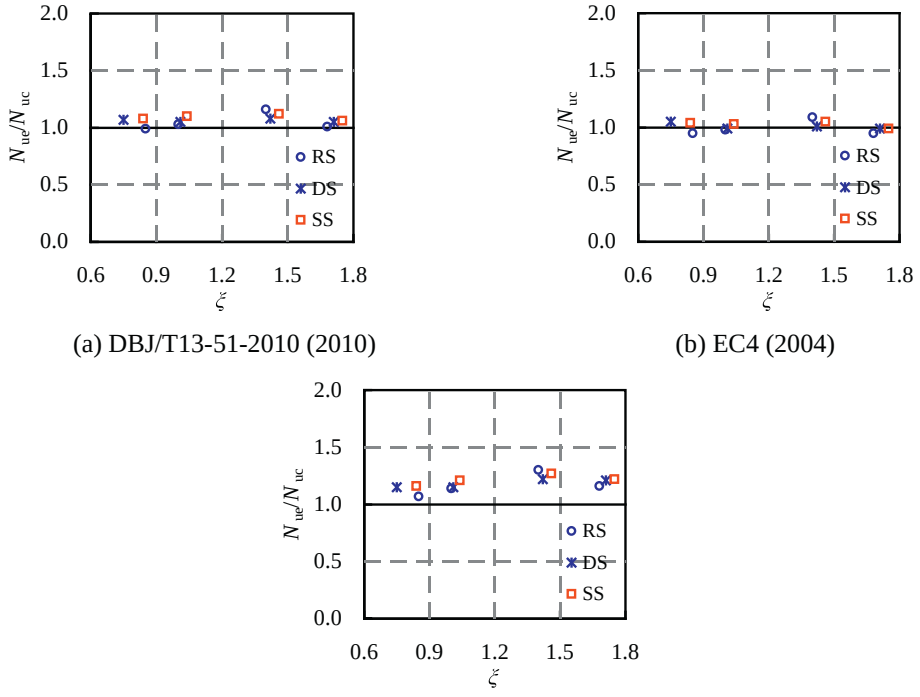

(a) DBJ/T13-51-2010 (2010)

(b) EC4 (2004)

(c) ANSI/AISC 360-10 (2010)

Fig. 15. Comparison between the measured and predicted capacities of circular CFSST specimens.

Table 5
Comparisons between the measured and predicted ultimate sectional capacity of square CFSSTs.

Specimen label	N_{ue} (kN)	DBJ/T13-51-2010 (2010)		EC4 (2004)		ANSI/AISC 360–10 (2010)	
		N_{DBJ} (kN)	N_{ue}/N_{DBJ}	N_{EC4} (kN)	N_{ue}/N_{EC4}	N_{ASIC} (kN)	N_{ue}/N_{ASIC}
S-3-L-RS-1	1461.5	1616.0	0.90	1498.5	0.98	1427.1	1.02
S-3-L-RS-2	1534.1	1616.0	0.95	1498.5	1.02	1427.1	1.07
S-3-H-RS-1	1584.9	1738.6	0.91	1595.1	0.99	1536.5	1.03
S-3-H-RS-2	1532.8	1738.6	0.88	1595.1	0.96	1536.5	1.00
S-4-L-RS-1	2039.6	1824.2	1.12	1681.2	1.21	1630.6	1.25
S-4-L-RS-2	1930.6	1824.2	1.06	1681.2	1.15	1630.6	1.18
S-5-H-RS-1	2124.6	2114.1	1.00	1943.0	1.09	1879.9	1.13
S-5-H-RS-2	2011.9	2114.1	0.95	1943.0	1.04	1879.9	1.07
S-3-L-DS-1	1543.3	1621.1	0.95	1502.5	1.03	1431.5	1.08
S-3-L-DS-2	1590.0	1621.1	0.98	1502.5	1.06	1431.5	1.11
S-3-H-DS-1	1768.8	1852.5	0.95	1684.8	1.05	1644.1	1.08
S-3-H-DS-2	1913.8	1852.5	1.03	1684.8	1.14	1644.1	1.16
S-4-L-DS-1	1955.4	1830.2	1.07	1685.8	1.16	1635.1	1.20
S-4-L-DS-2	1896.5	1830.2	1.04	1685.8	1.12	1635.1	1.16
S-5-L-DS-1	2151.5	2120.1	1.01	1947.5	1.10	1884.3	1.14
S-5-L-DS-2	2141.3	2120.1	1.01	1947.5	1.10	1884.3	1.14
S-3-L-SS-1	1724.6	1671.5	1.03	1542.3	1.12	1475.9	1.17
S-3-L-SS-2	1780.0	1671.5	1.06	1542.3	1.15	1475.9	1.21
S-3-H-SS-1	1689.7	1754.6	0.96	1607.7	1.05	1551.3	1.09
S-3-H-SS-2	1765.1	1754.6	1.01	1607.7	1.10	1551.3	1.14
S-4-L-SS-1	2007.7	1881.6	1.07	1725.2	1.16	1680.3	1.19
S-4-L-SS-2	1947.0	1881.6	1.03	1725.2	1.13	1680.3	1.16
S-5-L-SS-1	2215.0	2171.5	1.02	1986.0	1.12	1928.7	1.15
S-5-L-SS-2	2196.8	2171.5	1.01	1986.0	1.11	1928.7	1.14
Mean		1.00		1.09		1.13	
Standard deviation		0.06		0.06		0.06	

calculated results by AISC-360-10 (2010) and DBJ/T13-51-2010 (2010) are conservative, whilst those predicted by EC4 (2004) are also conservative yet closer to the measured results. When using DBJ/T13-51-2010 (2010), the mean value of N_{ue}/N_{uc} is 1.07 with a standard deviation of 0.05; for AISC-360-10 (2010), the mean value of N_{ue}/N_{uc} is 1.19 with a standard deviation of 0.07; when EC4 (2004) is adopted, the mean value of N_{ue}/N_{uc} is 1.01 with a standard deviation of 0.05. As can be seen, the calculation results in accordance with all three codes of practice are acceptable to be used in design.

For square CFSST specimens, the calculated N_{uc} values are listed and compared with N_{ue} in Table 5. Comparison of the N_{ue}/N_{uc} ratios against the confinement effect coefficient ξ are shown in Fig. 16. As can be seen, for square CFSST, the calculated results by all three standards are conservative to the test results compared with the predictions of circular ones. Specifically, when using DBJ/T13-51-2010 (2010), the mean value of N_{ue}/N_{uc} is 1.00 with a standard deviation of 0.06; for EC4 (2004), the mean values of N_{ue}/N_{uc} are both 1.09 with a standard deviation of 0.06; for AISC-360-10 (2010), the mean value of N_{ue}/N_{uc} is 1.13 with a standard deviation of 0.06. From the above comparisons, it can be concluded that the three existing specifications for conventional carbon steel CFST with river sand concrete infill can provide reasonable predictions for the sectional capacity of sea sand CFSST stub columns.

6. Conclusions

In the present study, a total of 48 circular and square sea sand concrete-filled stainless steel tube specimens were experimentally investigated with their main structural parameters varied. The following conclusions can be drawn based on the test results and analysis,

(1) Generally speaking, sea sand CFSST specimens showed excellent ductility during the axial compression tests. The failure modes of such type of innovative composite columns were outward local buckling at the mid-height for circular CFSST and outward buckling in wave pattern for square ones, i.e., similar with those of conventional river sand concrete-filled carbon steel tubes. No distinct detrimental effects were observed when using sea sand in the concrete mixture.
(2) The behaviour and sectional capacity of sea sand CFSST columns were significantly influenced by the confinement factor and the concrete strength. The strength and the strain development

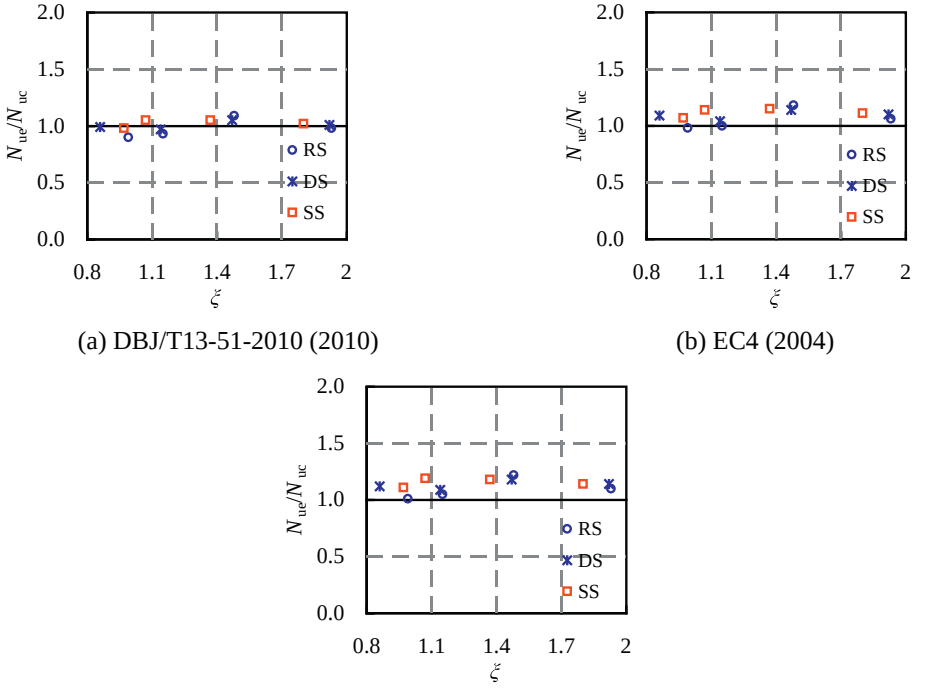

(a) DBJ/T13-51-2010 (2010)

(b) EC4 (2004)

(c) ANSI/AISC 360-10 (2010)

Fig. 16. Comparison between the measured and predicted capacities of square CFSST specimens.

results indicated that the confinement effects of stainless steel tube on sea sand concrete were as reliable as those on conventional river sand concrete.

(3) Compared with CFSST columns with river sand core concrete, those with both desalted sea sand concrete and sea sand concrete would lead to a certain decrease of ductility. However, with the increase of steel ratio or decrease of concrete strength, the confinement effects of stainless steel tube would be enhanced to reduce the detrimental effects of sea sand concrete in terms of ductility.

(4) Three existing codes on conventional CFST columns, AISC360–10, EC4 and DBJ/T13-51-2010, were tentatively adopted to predict the ultimate sectional capacity of the tested sea sand CFSST columns. All these design specifications provide generally conservative yet reasonable predictions.

The results obtained from the current testing program have indicated the feasibility of sea sand CFSST columns under short-term axial compressive loading. It should be noted that further investigations are needed to evaluate the structural behaviour of sea sand CFSST under complex loading conditions and long-term loading conditions.

Acknowledgements

The authors gratefully acknowledge the financial support provided by the National Natural Science Foundation of China (No. 51578154) and Fujian Provincial Department of Science and Technology (No. 2018H6005). This research is also part of International Collaborative Research Project of Fujian Agriculture and Forestry University (No. KXGH17009).

References

[1] L.H. Han, W. Li, R. Bjorhovde, Developments and advanced applications of concrete-filled steel tubular (CFST) structures: members, J. Constr. Steel Res. 100 (2014) 211–228.
[2] E. Ellobody, B. Young, Nonlinear analysis of concrete-filled steel SHS and RHS columns, Thin-Walled Struct. 44 (2006) 919–930.
[3] D.M. Denavit, Characterization of Behavior of Steel-Concrete Composite Members and Frames with Applications for Design, Ph.D. Dissertation University of Illinois at Urbana-Champaign, Urbana, 2012.
[4] M. Johansson, M. Akesson, Finite element study of concrete-filled steel tubes using a new confinement-sensitive concrete compression model, Nordic Concr. Res. 27 (2001) 43–62.
[5] J.Y. Zhu, T.M. Chan, Experimental investigation on octagonal concrete filled steel stub columns under uniaxial compression, J. Constr. Steel Res. 147 (2018) 457–467.
[6] E. Ellobody, B. Young, D. Lam, Behaviour of normal and high strength concrete-filled compact steel tube circular stub columns, J. Constr. Steel Res. 62 (2006) 706–715.
[7] L.H. Han, G.H. Yao, X.L. Zhao, Tests and calculations for hollow structural steel (HSS) stub columns filled with self-consolidating concrete (SCC), J. Constr. Steel Res. 61 (2005) 1241–1269.
[8] Y. Li, X. Zhao, R.R. Singh, S. Al-Saadi, Experimental study on seawater and sea sand concrete filled GFRP and stainless steel tubular stub columns, Thin-Walled Struct. 106 (2016) 390–406.
[9] T.M. Chan, Y.M. Huai, Experimental investigation on lightweight concrete-filled cold-formed elliptical hollow section stub columns, J. Constr. Steel Res. 115 (2015) 434–444.
[10] B.N.N. Kumar, P.K. Kumar, E.R. Babu, M. Gopal, D.S. Reddy, K. Sreekanth, U. Yellppa, An experimental study on sea sand by partial replacement of sea sand in concrete, Int. J. Sci. Res. Sci. Technol. 2 (2016) 181–184.
[11] H.G. Yin, Y. Li, H.L. Lv, Q. Gao, Durability of Sea-Sand Containing Concrete: Effects of Chloride Ion Penetration, vol. 21, Mining Science and Technology, 2011 123–127 (in Chinese).
[12] N. Baddoo, Stainless steel in construction: a review of research, applications, challenges and opportunities, J. Constr. Steel Res. 64 (2008) 1199–1206.
[13] L.H. Han, C.Y. Xu, Z. Tao, Performance of concrete filled stainless steel tubular (CFSST) columns and joints: Summary of recent research, J. Constr. Steel Res. (2018), https://doi.org/10.1016/j.jcsr.2018.02.038.
[14] Z. Tao, B. Uy, F.Y. Liao, L.H. Han, Nonlinear analysis of concrete-filled square stainless steel stub columns under axial compression, J. Constr. Steel Res. 67 (2011) 1719–1732.
[15] B. Uy, Z. Tao, L.H. Han, Behaviour of short and slender concrete-filled stainless steel tubular columns, J. Constr. Steel Res. 67 (2011) 360–378.
[16] D. Lam, L. Gardner, Structural design of stainless steel concrete filled columns, J. Constr. Steel Res. 64 (2008) 1275–1282.
[17] V.W. Tam, Z.B. Wang, Z. Tao, Behaviour of recycled aggregate concrete filled stainless steel stub columns, Mater. Struct. 47 (2014) 293–310.
[18] W.M. Quach, J.G. Teng, K.F. Chung, Three-stage full-range stress-strain model for stainless steels, J. Struct. Eng. ASCE 134 (2008) 1518–1527.
[19] B. Young, E. Ellobody, Experimental investigation of concrete-filled cold formed high strength stainless steel tube columns, J. Constr. Steel Res. 62 (2006) 484–492.
[20] F.Y. Liao, L.H. Han, Z. Tao, K.J.R. Rasmussen, Experimental behavior of concrete filled stainless steel tubular columns under laterally cyclic loading, J. Struct. Eng. ASCE 143 (2017) (04016219).
[21] Y. Chen, K. Wang, R. Feng, K. He, L.P. Wang, Flexural behavior of concrete-filled stainless steel CHS subjected to static loading, J. Constr. Steel Res. 139 (2017) 30–43.
[22] W.B. Zhou, Y. Chen, K. Wang, S.H. Han, F.P. Galarza, Experimental research on circular concrete filled stainless steel tubular truss, Thin-Walled Struct. 117 (2017) 224–238.
[23] V.I. Patel, Q.Q. Liang, M.N.S. Hadi, Nonlinear analysis of circular high strength concrete-filled stainless steel tubular slender beam-columns, Eng. Struct. 130 (2017) 1–13.
[24] M.F. Hassanein, M. Elchalakani, V.I. Patel, Overall buckling behaviour of circular concrete-filled dual steel tubular columns with stainless steel external tubes, Thin-Walled Struct. 115 (2017) 336–348.
[25] GB/T228.1–2010, Metallic Materials-Tensile Testing-Part1: Method of Test at Room Temperature, China Standard Press, Beijing, 2010.
[26] K.J.R. Rasmussen, Full-range stress - strain curves for stainless steel alloys, J. Constr. Steel Res. 59 (2003) 47–61.
[27] GB/T 14684-2011, Sand for Construction, General Administration of Quality Supervision, Inspection and Quarantine of the People's Republic of China, Beijing, 2011.
[28] JGJ52-2006, Standard for Technical Requirements and Test Method of Sand and Crushed Stone (or Gravel) for Ordinary Concrete, Ministry of Construction of the People's Republic of China, Beijing, 2006.
[29] Z. Tao, L.H. Han, Z.B. Wang, Experimental behaviour of stiffened concrete-filled thin-walled hollow steel structural (HSS) stub columns, J. Constr. Steel Res. 61 (2005) 962–983.
[30] ANSI/AISC 360–10, Specification for Structural Steel Buildings, American Institute of Steel Construction, Chicago (IL,USA), 2010.
[31] DBJ/T 13-51-2010, Technical Specification for Concrete-Filled Steel Tubular Structures, The Department of Housing and Urban-Rural Development of Fujian Province, Fuzhou (China), 2010.
[32] Eurocode 4. EN 1994-1-1, Design of Composite Steel and Concrete Structures - Part 1-1: GENERAL Rules and Rules for Buildings, European Committee for Standardization, Brussels, 2004 (2004).